The EMBO Journal (2008) 27, 1345–1356 | © 2008 European Molecular Biology Organization | All Rights Reserved 0261-4189/08
www.embojournal.org

THE EMBO JOURNAL

Activation of TRPP2 through mDia1-dependent voltage gating

Chang-Xi Bai[1], Sehyun Kim[1], Wei-Ping Li[1,3], Andrew J Streets[2], Albert CM Ong[2] and Leonidas Tsiokas[1,*]

[1]Department of Cell Biology, University of Oklahoma Health Sciences Center, Oklahoma City, OK, USA and [2]Kidney Genetics Group, Academic Nephrology Unit, The Henry Wellcome Laboratories for Medical Research, School of Medicine and Biomedical Sciences, University of Sheffield, Sheffield, UK

The TRPP2 cation channel is directly responsible for ~15% of all cases of autosomal dominant polycystic kidney disease. However, the mechanisms underlying fundamental properties of TRPP2 regulation, such as channel gating and activation, are unknown. We have shown that TRPP2 was activated by EGF and physically interacted with the mammalian diaphanous-related formin 1 (mDia1), a downstream effector of RhoA. Now, we show that mDia1 regulates TRPP2 by specifically blocking its activity at negative but not positive potentials. The voltage-dependent unblock of TRPP2 by mDia1 at positive potentials is mediated through RhoA-induced molecular switching of mDia1 from its autoinhibited state at negative potentials to its activated state at positive potentials. Under physiological resting potentials, EGF activates TRPP2 by releasing the mDia1-dependent block through the activation of RhoA. Our data reveal a new role of mDia1 in the regulation of ion channels and suggest a molecular basis for the voltage-dependent gating of TRP channels.

The EMBO Journal (2008) **27,** 1345–1356. doi:10.1038/emboj.2008.70; Published online 3 April 2008
Subject Categories: signal transduction; molecular biology of disease
Keywords: autosomal dominant polycystic kidney disease; mDia1; RhoA; TRP channels; TRPP2

Introduction

TRPP2 (polycystin-2 or PKD2) is the protein product of the *pkd2* gene originally identified as one of the genes responsible for autosomal dominant polycystic kidney disease (Mochizuki *et al*, 1996). Structurally, it belongs to the TRP superfamily of channel proteins (Nilius *et al*, 2007; Venkatachalam and Montell, 2007) and possesses channel activity (Hanaoka *et al*, 2000; Gonzalez-Perrett *et al*, 2001; Vassilev *et al*, 2001; Koulen *et al*, 2002; Luo *et al*, 2003; Delmas *et al*, 2004; Ma *et al*, 2005), which mediates all of its biological functions (Cantiello, 2004; Tsiokas *et al*, 2007). However, some of the very basic biophysical properties of TRPP2, such as gating and activation, remain completely unknown. Recent study on a subset of TRP channels activated mainly by temperature has shown that voltage-dependent gating underlies their activation mechanism (Voets *et al*, 2004; Nilius *et al*, 2005). Current data on the voltage-dependent gating of TRPP2 are quite controversial depending on the cell or cell-free system used. *In vitro*-reconstituted TRPP2 derived from various sources such as endoplasmic reticulum endomembranes (Koulen *et al*, 2002), Sf9 insect plasma membranes, apical membranes of syncytiotrophoblasts (Gonzalez-Perrett *et al*, 2001, 2002) or *in vitro*-translated TRPP2 (Gonzalez-Perrett *et al*, 2001) showed strong voltage dependence with high activity at negative potentials and almost no activity at positive potentials. In sharp contrast, native TRPP2 displayed voltage dependence with higher activity at positive potentials (Luo *et al*, 2003; Pelucchi *et al*, 2006; Kim *et al*, 2008) and overexpressed TRPP2 alone or in association with PKD1 did not show voltage dependence (Hanaoka *et al*, 2000; Delmas *et al*, 2004; Ma *et al*, 2005). It has been proposed that voltage-dependent gating of TRPP2 could be an intrinsic property of the channel, but it should be greatly modulated by protein–protein interactions under physiological conditions (Gonzalez-Perrett *et al*, 2001; Cantiello, 2004).

TRPP2 activation was shown to occur in response to EGFR activation in the kidney epithelial cell line, LLC-PK1 (Ma *et al*, 2005). The physiological relevance of EGF-induced activation of TRPP2 in LLC-PK1 cells was supported by whole animal studies whereby homozygous deletion of *egfr* resulted in cystic dilatation of collecting ducts (Threadgill *et al*, 1995), an area that was also predominantly affected by *pkd2* mutations (Wu *et al*, 2000). Mechanistically, TRPP2 overexpression increased EGF-induced conductance in LLC-PK1 kidney epithelial cells, whereas knock down of endogenous TRPP2 by RNA interference (RNAi) or expression of the pathogenic, missense variant, TRPP2-D511V, blunted the EGF-induced response (Ma *et al*, 2005). Pharmacological experiments indicated that the EGF-induced activation of TRPP2 occurred independently of store depletion but required the activity of phospholipase C (PLC) and phosphoinositide 3-kinase (PI3K) (Ma *et al*, 2005). Pipette infusion of purified phosphatidylinositol-4,5-bisphosphate (PIP_2) suppressed the TRPP2-mediated effect on EGF-induced conductance, whereas pipette infusion of phosphatidylinositol-3,4,5-trisphosphate (PIP_3) did not have any effect on this conductance (Ma *et al*, 2005). Overexpression of type Iα phosphatidylinositol-4-phosphate 5-kinase (PIP(5)Kα), which catalyses the formation of PIP_2, suppressed EGF-induced TRPP2 currents (Ma *et al*, 2005). Overall, TRPP2 functioned downstream of EGFR activation in LLC-PK1 cells.

*Corresponding author. Department of Cell Biology, University of Oklahoma Health Sciences Center, 975 NE 10th str, BRC1/262, Oklahoma City, OK 73104, USA. Tel.: +01 405 271 8001 ext 46211; Fax: +01 405 271 3758; E-mail: leonidas-tsiokas@ouhsc.edu
[3]Present address: Department of Pharmacology, Anhui Medical University, Hefei, Anhui Province 230032, People's Republic of China

Received: 31 October 2007; accepted: 14 March 2008; published online: 3 April 2008

In a yeast two-hybrid screen using the C-terminal tail of TRPP2, we identified mammalian diaphanous-related formin 1 (mDia1) as an interacting partner (Rundle *et al*, 2004). mDia1 functions downstream of RhoA in signal transduction, cytoskeletal organization, and cell cycle regulation (Wallar and Alberts, 2003; Gundersen *et al*, 2004; Higgs, 2005; Narumiya and Yasuda, 2006). Inactive or autoinhibited mDia1 exists in a 'closed' conformational state, whereby the diaphanous autoregulatory domain (DAD) at its C terminus loops around to bind the diaphanous inhibitory domain (DID) at its N terminus (Watanabe *et al*, 1999; Lammers *et al*, 2005; Otomo *et al*, 2005; Rose *et al*, 2005). Activated, GTP-bound Rho proteins (RhoA-C) bind to a G (for GTPase binding) domain, which is in close proximity to DID and relieves inhibition by DAD resulting in activation of mDia1. Activated mDia1 assumes an 'open' conformation, exposing formin homology 1 and 2 (FH1 and FH2) domains for interaction with several downstream effector molecules.

In the present study, we show that mDia1 functioned as an intracellular, voltage-dependent regulator of TRPP2. At resting potentials, autoinhibited mDia1 bound to and blocked TRPP2, whereas at positive potentials activated mDia1 released the block on TRPP2 leading to channel activation. EGF or membrane depolarization activated TRPP2 through the sequential activation of RhoA and mDia1. The voltage-dependent block of TRPP2 by mDia1 served two physiologically relevant roles, to underlie the activation mechanism of TRPP2 by EGF and to set the resting membrane potential of kidney epithelial cells to its resting value by preventing constitutive activation of TRPP2.

Results

Colocalization of native TRPP2 and mDia1 in the plasma membrane of kidney epithelial cells

Although TRPP2 has been shown to be present in the plasma membrane of a variety of cell types, including MDCK (Scheffers *et al*, 2002), mIMCD3 (Luo *et al*, 2003), HEK293 (Pelucchi *et al*, 2006), and human syncytiotrophoblasts (Gonzalez-Perrett *et al*, 2001), its presence in the plasma membrane of LLC-PK1 cells has been questionable (Koulen *et al*, 2002; Luo *et al*, 2003). Immunofluorescence staining of endogenous TRPP2 in LLC-PK1 cells using a commercially available antibody (G20; Santa Cruz Biotechnology Inc.) revealed consistent staining in the plasma membrane (Figure 1A and D), as was previously shown for MDCK and mIMCD3 cells (Li *et al*, 2005a). G20 detected native and transfected TRPP2 (Figure 1C). Plasma membrane staining was specific to TRPP2, as it was eliminated in cells treated with the glycogen synthase kinase 3 (GSK3) inhibitor (Figure 1B), SB 415286, which was shown to inhibit the GSK3-dependent N-terminal phosphorylation of TRPP2 necessary for its targeting to the plasma membrane in MDCK cells (Streets *et al*, 2006). To determine whether mDia1 colocalized with TRPP2 at the plasma membrane, native LLC-PK1 cells were double stained with G20 (α-TRPP2) and a mouse monoclonal antibody against mDia1. Figure 1D–F shows that both proteins colocalized at the plasma membrane. Transfected TRPP2 was also detected at the plasma membrane and its expression there was not altered by transfected mDia1 (Supplementary Figure S1). Altogether, these data led us to conclude that endogenous or transfected

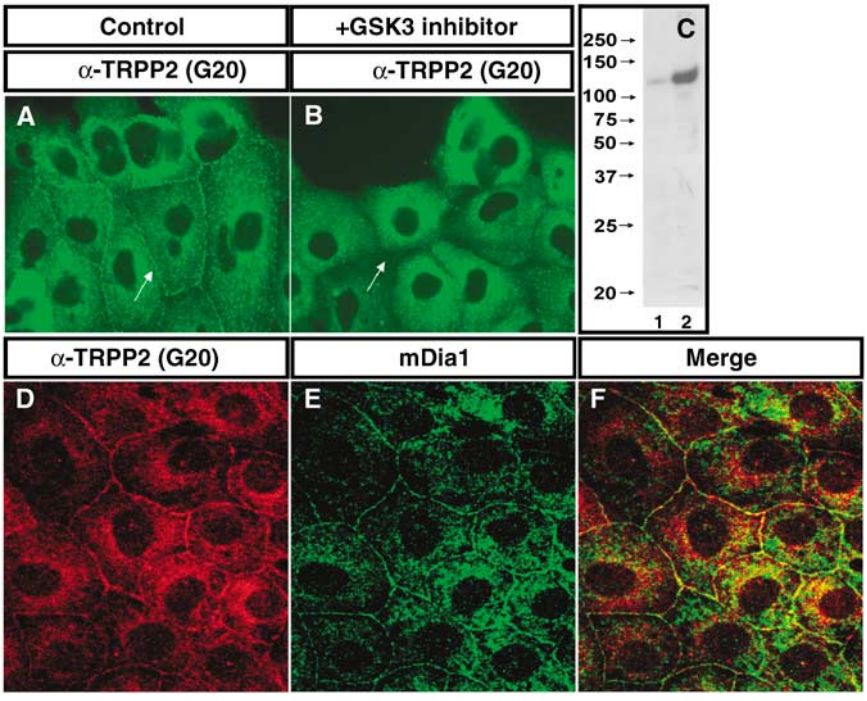

Figure 1 Colocalization of mDia1 and TRPP2 at the plasma membrane of LLC-PK1 cells. Expression of endogenous TRPP2 in untreated LLC-PK1 cells (**A**) or cells treated with the GSK3 inhibitor, SB 415286 (40 μM) for 16 h (**B**). (**C**) Detection of endogenous (lane 1) or transfected TRPP2 (lane 2) in lysates (75 μg) of LLC-PK1 cells by α-TRPP2 (1:300, G20; Santa Cruz Biotechnology Inc.). (**D**–**F**) Cell surface colocalization of native TRPP2 and mDia1 in LLC-PK1 cells. TRPP2 was stained with G20 (1:50) (D) and mDia1 with a mouse monoclonal (1:500) (E). Overlay is shown in (F).

TRPP2 was expressed in a significant amount at the plasma membrane of LLC-PK1 cells where it colocalized with mDia1. mDia1 did not affect TRPP2 trafficking to and/or from the plasma membrane.

Voltage-dependent regulation of TRPP2 by mDia1 in native LLC-PK1 cells

Next, we measured whole cell background currents in native LLC-PK1 cells. Cells were held at −60 mV and bathed in normal tyrode solution. Under these conditions, an outwardly rectifying current was recorded in native LLC-PK1 cells (Figure 2A and B). To determine whether native TRPP2 contributed to this current, we employed two independent loss-of-function experiments. First, LLC-PK1 cells were transiently transfected with a single-point mutant form of TRPP2 (TRPP2-D511V). This mutant lacks channel activity (Koulen *et al*, 2002; Ma *et al*, 2005; Li *et al*, 2005b) and behaves as a dominant-negative interfering allele (Ma *et al*, 2005) by binding up wild-type TRPP2 (Supplementary Figure S2A, lane 2). Second, LLC-PK1 cells were dialysed through pipette infusion with a rabbit TRPP2-specific affinity-purified antibody (α-TRPP2) which has been shown previously to neutralize TRPP2 activity (Ma *et al*, 2005). Transfection of TRPP2-D511V (Figure 2C and D) or pipette infusion of α-TRPP2, but not control IgG (Supplementary Figure S2B–E) reduced both inward and outward background whole cell currents. However, the effect was more pronounced at positive potentials (Supplementary Figure S2D and E), indicating that native TRPP2 contributed to an outwardly rectifying current. Next, we tested the role of endogenous mDia1 on

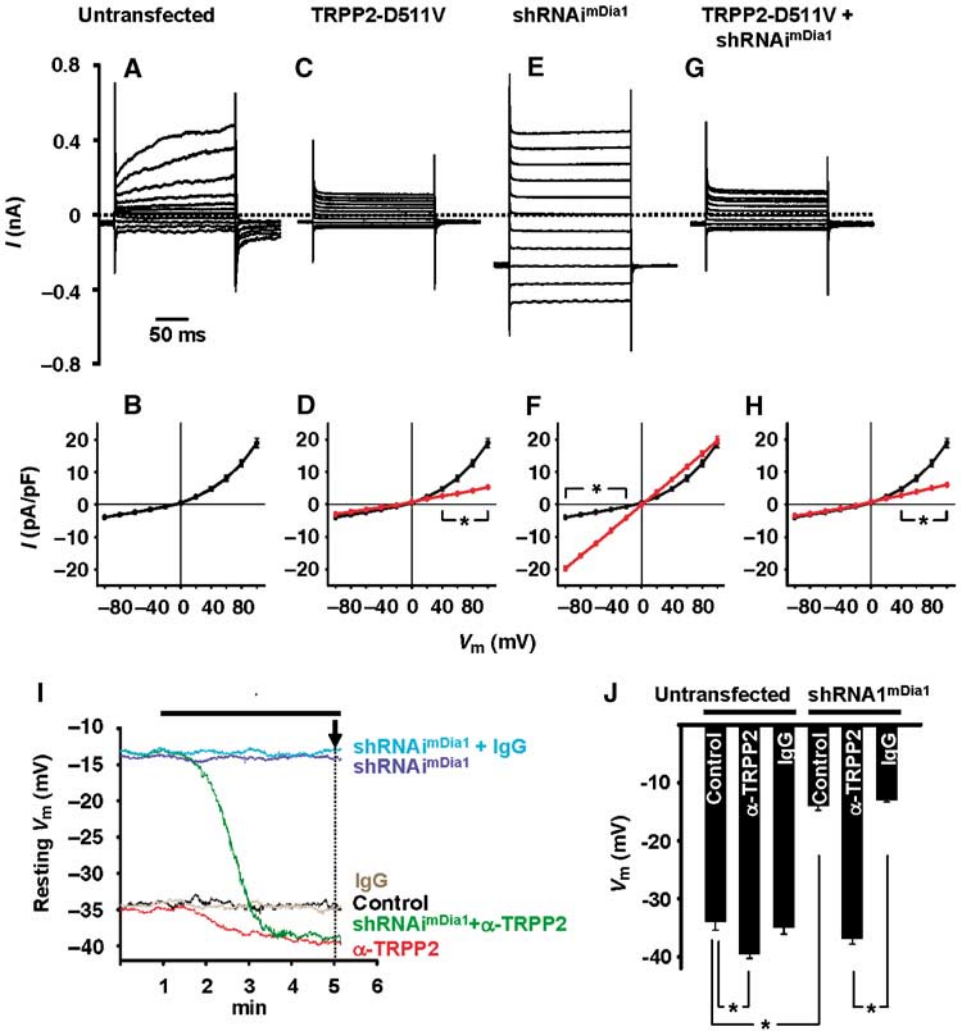

Figure 2 Voltage-dependent block of endogenous TRPP2 by mDia1 in LLC-PK1 cells. (**A**–**H**) Step currents and pooled current–voltage (I–V) curves in normal tyrode extracellular solution in native LLC-PK1 (untransfected, $n=9$) (A, B), TRPP2-D511V-transfected LLC-PK1 cells (TRPP2-D511V, $n=8$) (C, D), shRNAi^{mDia1}-transfected cells (shRNAi^{mDia1}, $n=8$) (E, F), or TRPP2-D511V plus shRNAi^{mDia1}-doubly transfected cells (TRPP2-D511V plus shRNAi^{mDia1}, $n=7$) (G, H). Pooled I–V curve derived from native LLC-PK1 cells (B) is shown in black for comparison (D, F, and H). $^*P<0.05$. Parentheses indicate a range of membrane potentials at which there was a significance difference in current density between native and transfected cells. (**I**, **J**) Time-dependent effect of α-TRPP2 (200 ng/ml) dialysis on the mean resting membrane potential (mV) of untransfected LLC-PK1 ($n=7$) (red) or cells transfected with an shRNAi^{mDia1} construct targeting pig mDia1 ($n=7$) (green). Normal rabbit IgG (200 ng/ml) dialysed into untransfected LLC-PK1 (grey) ($n=7$) or shRNAi^{mDia1}-transfected cells (light blue) ($n=6$) was used as a negative control. Resting membrane potential of untransfected LLC-PK1 cells or cells transfected with shRNAi^{mDia1} is shown as control (black) ($n=7$) or shRNAi^{mDia1} (dark blue) ($n=7$), respectively. Values of resting membrane potentials 5 min after break-in (arrow) were used for statistical analysis shown in (J).

native currents and its functional interaction with TRPP2. We designed an shRNAi construct to target porcine mDia1 (shRNAi^{mDia1}). The silencing efficiency of such a construct is shown in Supplementary Figure S2F. Knocking down mDia1 increased mainly inward currents (Figure 2E and F), whereas double transfection of TRPP2-D511V and shRNAI^{mDia1} suppressed both inward and outward currents to levels seen with TRPP2-D511V alone (Figure 2G and H). These data showed that endogenous mDia1 blocked TRPP2-mediated inward, but not outward currents. Therefore, native TRPP2 alone or in association with other channel subunits was under voltage-dependent regulation by mDia1 in LLC-PK1 cells.

To provide independent evidence for the mDia1-dependent block of TRPP2 in native LLC-PK1 cells, we tested whether it regulated the membrane potential of LLC-PK1 cells by preventing constitutive activation of TRPP2 and ensuing depolarization. Figure 2I and J shows that pipette infusion of α-TRPP2 (red), but not control IgG (grey) produced a time-dependent hyperpolarization of LLC-PK1 cells. In contrast, knock down of pig mDia1 resulted in significant depolarization (dark blue). Pipette infusion of α-TRPP2 into cells lacking mDia1 reversed the depolarization to hyperpolarization (green) to a level almost identical to the level caused by TRPP2 inhibition in cells with normal levels of mDia1 (red). These data verified the mDia1-dependent block of TRPP2 using an independent approach and provided evidence for an important physiological role of the mDia1–TRPP2 interaction in setting the membrane potential of these cells to its resting level.

Voltage-mediated regulation of TRPP2 through mDia1 activation

To understand the mechanism by which mDia1 blocked TRPP2 activity at negative potentials, but not at positive potentials, we employed overexpression experiments in LLC-PK1 cells. Massive (>10-fold) overexpression of TRPP2 in LLC-PK1 cells either by stable expression (LLC-PK1^{TRPP2} cells) (Ma *et al*, 2005) or transient transfection from a strong mammalian promoter (cytomegalovirus promoter, pCDNA3-based vectors, data not shown) resulted in the formation of a constitutively active channel with no obvious signs of any type of voltage dependence (Figure 3A and B). In addition, overall increase in whole cell outward currents was ~50% (from 18.9 ± 1.4 pA/pF in LLC-PK1 cells ($n=9$) to 28.6 ± 0.6 pA/pF in LLC-PK1^{TRPP2} cells ($n=9$) at -100 mV) (Figure 3B), despite massive overexpression. To explain the lack of residual outward rectification and modest amplitude increase, we reasoned that TRPP2 could not form a functional channel by itself but it had to interact with additional subunits such as PKD1 (Tsiokas *et al*, 1997), TRPC1 (Tsiokas *et al*, 1999; Bai *et al*, 2008), TRPC4 (through an indirect interaction with TRPC1), and/or TRPV4 (Kottgen and Walz, 2005). Therefore, massive overexpression of just TRPP2 could alter the stoichiometry of native complexes and most importantly, strip mDia1 from these complexes. Monomeric TRPP2 bound to mDia1 should be non-functional, whereas TRPP2 associated with endogenous channel subunits should form functional complexes passing linear currents, as they would have lost regulation by mDia1. To provide evidence for this model, we expressed TRPP2 from the much weaker rat β-actin promoter (pJ6Ω expression plasmid, ATCC). Supplementary Figure S3A confirms that rat β-actin promoter was utilized less efficiently than the CMV promoter in LLC-PK1 cells, when the two promoters were compared side by side. Transfection of pJ6Ω-TRPP2 resulted in an amplification of native, outwardly rectifying currents (Supplementary Figure S3B–E), supporting the existence of a heteromultimeric channel complex of TRPP2 (Supplementary Figure S3F). We, therefore, proceeded with the LLC-PK1^{TRPP2} cells as an overexpression system, because it would allow us to add individual components (i.e. mDia1, RhoA constructs) and test whether linear TRPP2-mediated currents could be converted to outwardly rectifying currents.

Transient transfection of wild-type mDia1 (Figure 3C and D) into LLC-PK1^{TRPP2} cells suppressed both inward and outward currents, indicating that overexpression of the autoinhibited form of mDia1 was not sufficient to confer voltage sensitivity to TRPP2. Next, we examined whether activation of mDia1 could affect TRPP2 activity. Activation of mDia1 was achieved by co-transfection with constitutively active RhoA(V14), whereas dominant-negative RhoA(N19) was used as a negative control. Figure 3E and F shows that RhoA(N19) did not have an effect on mDia1-mediated block of TRPP2, whereas RhoA(V14) resulted in suppression of inward but not outward currents in LLC-PK1^{TRPP2} cells (Figure 3G and H), recapitulating native currents. Overexpression of RhoA(V14) in the absence of transfected mDia1 did not alter TRPP2-mediated currents (Figure 3I and J) confirming the role of mDia1 in TRPP2 regulation and also, the existence of a heteromultimeric complex of TRPP2 and other channel subunits (Supplementary Figure S3F). If TRPP2 associated with other channel subunits had retained some of native mDia1, massive expression of Rho(V14) should have resulted in some outward rectification, which was not the case. Confirmation that transfected mDia1 and RhoA(V14) acted through TRPP2 was obtained by the suppression of whole cell currents by cell dialysis of triple-transfected cells with α-TRPP2 (data not shown in normal tyrode solution, but shown in symmetrical K^+; Supplementary Figure S5E and F). Slight current activation (or relaxation) at depolarizing potentials was only noted in cells co-transfected with mDia1 and RhoA(V14) (Figure 3G), but not with any of the cells transfected with TRPP2 alone (Figure 3A), TRPP2/mDia1 (Figure 3C), TRPP2/mDia1/RhoA(N19) (Figure 3E), or TRPP2/RhoA(V14) (Figure 3I).

To test whether the activated mDia1-induced outward rectification (Figure 3G and H) was due to voltage-dependent gating of TRPP2, we employed a tail current protocol (Voets *et al*, 2004). Because, mDia1 was originally identified as an interacting partner of TRPP2 (Rundle *et al*, 2004), we hypothesized that activated mDia1 bound to and blocked TRPP2 activity at negative potentials, whereas it dissociated or 'swung away' from TRPP2 at positive potentials. Therefore, dissociation of activated mDia1 from TRPP2 should be manifested as time-dependent current relaxation at positive potentials, whereas protein re-association should be manifested as time-dependent current de-activation at hyperpolarizing potentials following a strong depolarizing pulse at 120 mV for 200 ms. Figure 3K–R shows that whole cell currents displayed current relaxation and de-activation (Figure 3O and P) in cells transfected with activated mDia1 but not in mDia1-untransfected cells (Figure 3K and L), cells transfected with autoinhibited mDia1 (Figure 3M and N), or

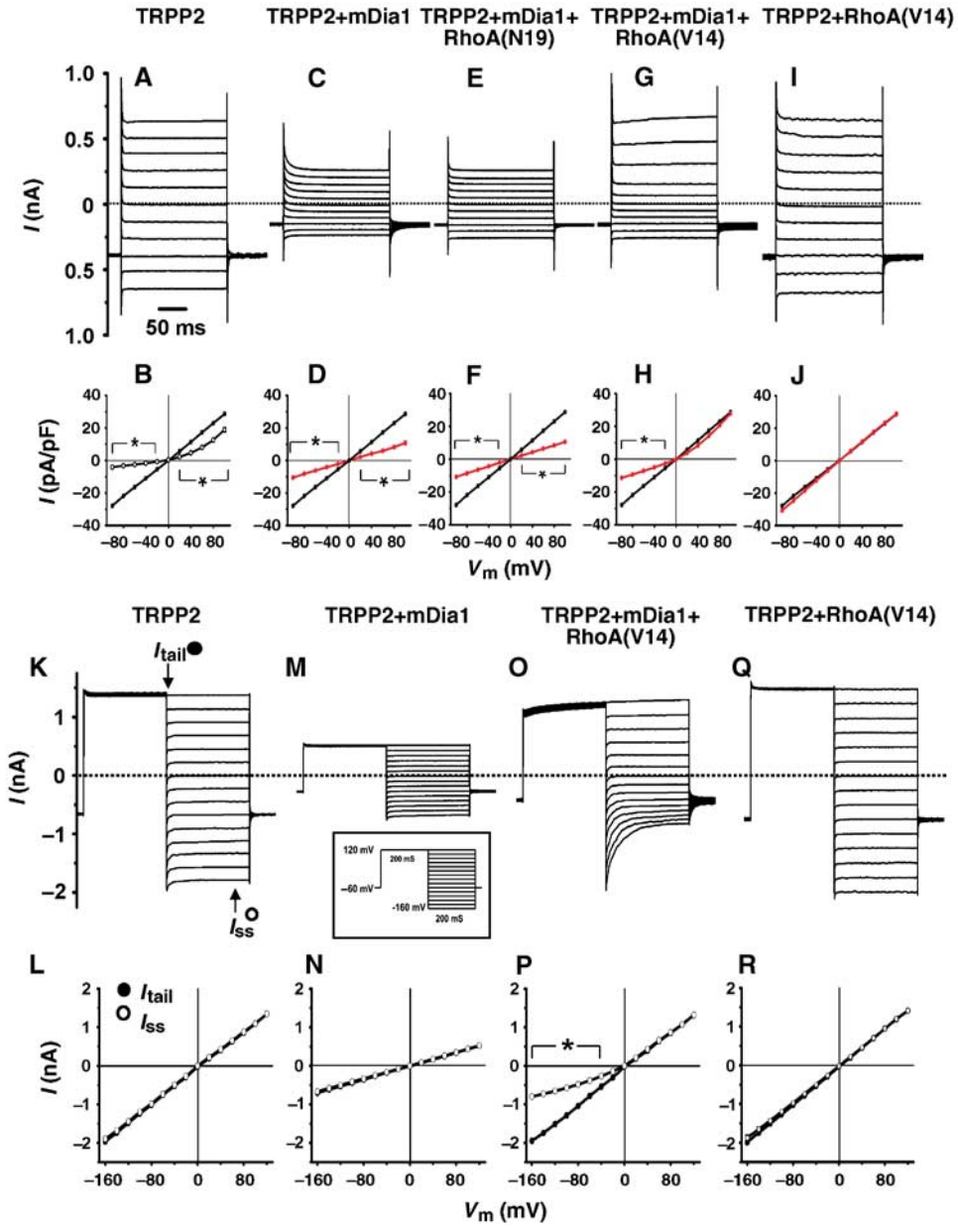

Figure 3 Voltage-dependent block of TRPP2 by activated mDia1. (**A–J**) Step currents and pooled I–V curve in normal tyrode extracellular solution in LLC-PK1^{TRPP2} cells (TRPP2, $n=9$) (A, B), LLC-PK1^{TRPP2} cells transiently transfected with mDia1 (TRPP2 + mDia1, $n=8$) (C, D), transiently co-transfected with mDia1 plus RhoA(N19) (TRPP2 + mDia1 + RhoA(N19), $n=8$) (E, F), mDia1 plus RhoA(V14) (TRPP2 + mDia1 + RhoA(V14), $n=8$) (G, H), or RhoA(V14) without mDia1 (TRPP2 + RhoA(V14), $n=7$) (I, J). Pooled I–V curve derived from untransfected LLC-PK1 cells (Figure 2B) is shown in open circles for comparison (B). Pooled I–V curve derived from LLC-PK1^{TRPP2} cells (B) is shown in black for comparison (D, F, H, and J). $^*P<0.05$. Parentheses indicate a range of membrane potentials at which there was a significance difference in current density between the two groups of cells. (**K–R**) Tail (I_{tail}) and steady-state currents (I_{ss}) in mDia1-untransfected (TRPP2, $C_m=22.7\pm0.4$ pF, $n=8$) (K, L), mDia1- (TRPP2 + mDia1, $C_m=22.8\pm0.4$ pF, $n=7$) (M, N), mDia1 plus RhoA(V14)-transfected (TRPP2 + mDia1 + RhoA(V14), $C_m=23.2\pm0.4$ pF, $n=7$) (O, P), or RhoA(V14)- (TRPP2 + RhoA(V14), $C_m=22.9\pm0.5$ pF, $n=7$) transfected LLC-PK1^{TRPP2} cells (Q, R). Tail-current protocol used to demonstrate the voltage-dependent gating of TRPP2 is shown in inset. $^*P<0.05$. Parentheses indicate a range of membrane potentials at which there was a significance difference between tail and steady-state currents within the same group.

RhoA(V14) alone (Figure 3Q and R). Similar data were obtained when K^+ was used as the sole charge carrier ruling out the possibility of divalent-induced rectification patterns in I–V curves (Supplementary Figures S4 and S5). Overall, these data led us to propose that activated mDia1 conferred voltage sensitivity to overexpressed TRPP2 in LLC-PK1 cells and supported data on native LLC-PK1 cells.

Structure–function analysis of mDia1

Next, we wished to provide a molecular basis for the voltage-dependent block of TRPP2 by mDia1 by identifying the minimal domain in mDia1 responsible for its effect on TRPP2 and also to confirm that activated constructs of mDia1 should confer voltage sensitivity to TRPP2 in the absence of activation through RhoA. Because TRPP2 showed

higher conductance in K^+ than Na^+ or Ca^{2+} (Luo *et al*, 2003; Ma *et al*, 2005) and also to avoid Ca^{2+}-induced rectifications, in these experiments we measured whole cell currents in symmetrical K^+. A series of N- and C-terminal truncation mutants and the mDia1(M1182A) mutant, which was shown to render mDia1 in the activated state (Lammers *et al*, 2005), were tested for their effect on TRPP2.

Transfection of the ΔN3mDia1 mutant, which lacked the TRPP2-binding site, was without effect (Figure 4A), whereas activated constructs mDia1(1–747) (Figure 4B), mDia1 (1–1144) (Figure 4C), or mDia1(M1182A) (Figure 4D) conferred outward rectification on TRPP2 currents. mDia1 (1–586) (Figure 4E) and mDia1(1–1203) (Figure 4F) behaved as wild-type mDia1 in the autoinhibited state. Construct mDia1(1–1169), which was expected to result in partial activation (Lammers *et al*, 2005), partially suppressed outward currents (Figure 4G). Tail current experiments in cells transfected with mDia1(1–586) and mDia1(1–1144) confirmed the voltage-dependent effect of activated mDia1 on TRPP2 currents (Supplementary Figure S6A–G). The voltage-dependent effect of activated forms of mDia1 such as mDia1(1–1144) was consistent with a Boltzmann distribution of mean conductance as a function of test potential (Figure 4H). Interestingly, partially activated mDia1(1–1169) showed a positive shift in $V_{1/2}$ by about 28 mV (from 11.7 ± 7.7 mV in mDia1(1–1144) to 39.8 ± 2.7 mV) and significantly lower G_{max} (from 10.0 ± 0.1 nS in mDia1(1–1144) to 5.4 ± 0.1 nS), indicating that the level of mDia1 activation

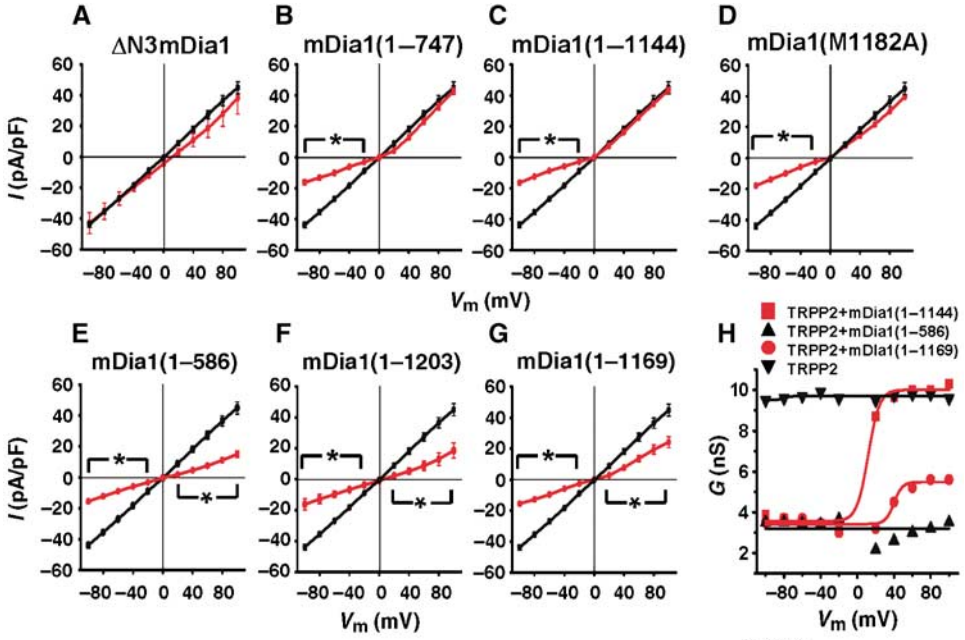

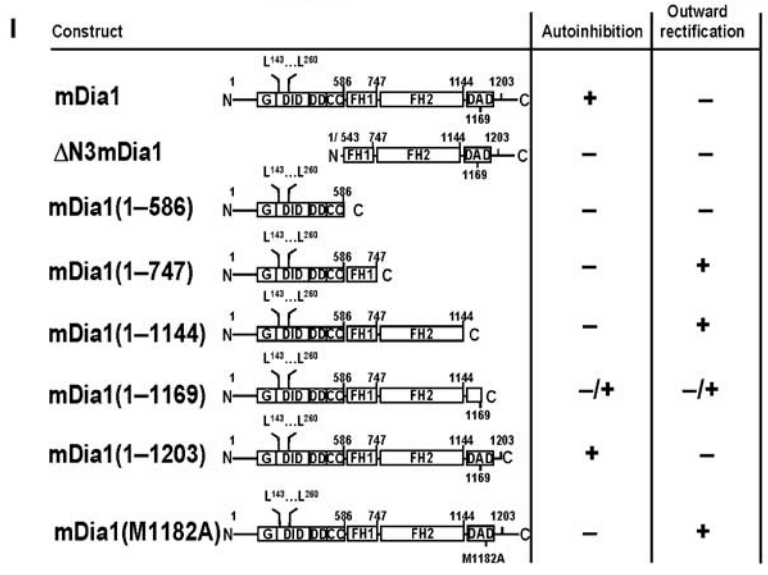

Figure 4 Structure–function analysis of mDia1. (**A**–**G**) Pooled I–V curves of LLC-PK1^{TRPP2} cells transfected with ΔN3mDia1 (A), mDia1(1–747) (B), mDia1(1–1144) (C), mDia1(M1182A) (D), mDia1(1–586) (E), mDia1(1–1203) (F), or mDia1(1–1169) (G). Pooled I–V curve derived from untransfected LLC-PK1^{TRPP2} cells (Figure 3B) is shown in black for comparison (A–G). *$P<0.05$. (**H**) Boltzmann distributions of mean conductance (G) derived from steady-state currents at the end of the pulse as a function of test potential (V_m). (**I**) Summary data of structure–function analysis of mDia1. CC, coiled-coil region; DAD, diaphanous autoregulatory domain; DD, dimerization domain; DID, diaphanous inhibitory domain; G, GTPase-binding region; FH1, formin homology 1 domain; FH2, formin homology 2 domain; L^{143}–L^{260}, TRPP2-binding domain.

dictated the voltage sensitivity of TRPP2. Summary data on structure-function analysis of mDia1 is shown in Figure 4I.

Direct voltage-dependent gating of TRPP2 by mDia1

To determine whether the mDia1-dependent voltage gating of TRPP2 was direct, recombinant mDia1(1–586) or mDia1 (1–747) (Figure 5A) was applied to the cytosolic side of inside-out patches excised from LLC-PK1^{TRPP2} cells. Time-course experiments indicated that 5 min starting perfusion of recombinant proteins was adequate to suppress TRPP2 inward currents (Figure 5B). Application of α-TRPP2 to the cytosolic side of excised patches of LLC-PK1^{TRPP2} cells confirmed the existence of functional TRPP2 by suppressing inward and outward macroscopic currents (Figure 5C–E). Application of normal rabbit IgG was without effect (Supplementary Figure S7A). Application of recombinant mDia1(1–586) suppressed macroscopic currents to levels identical to α-TRPP2 (Figure 5F–H) further confirming the

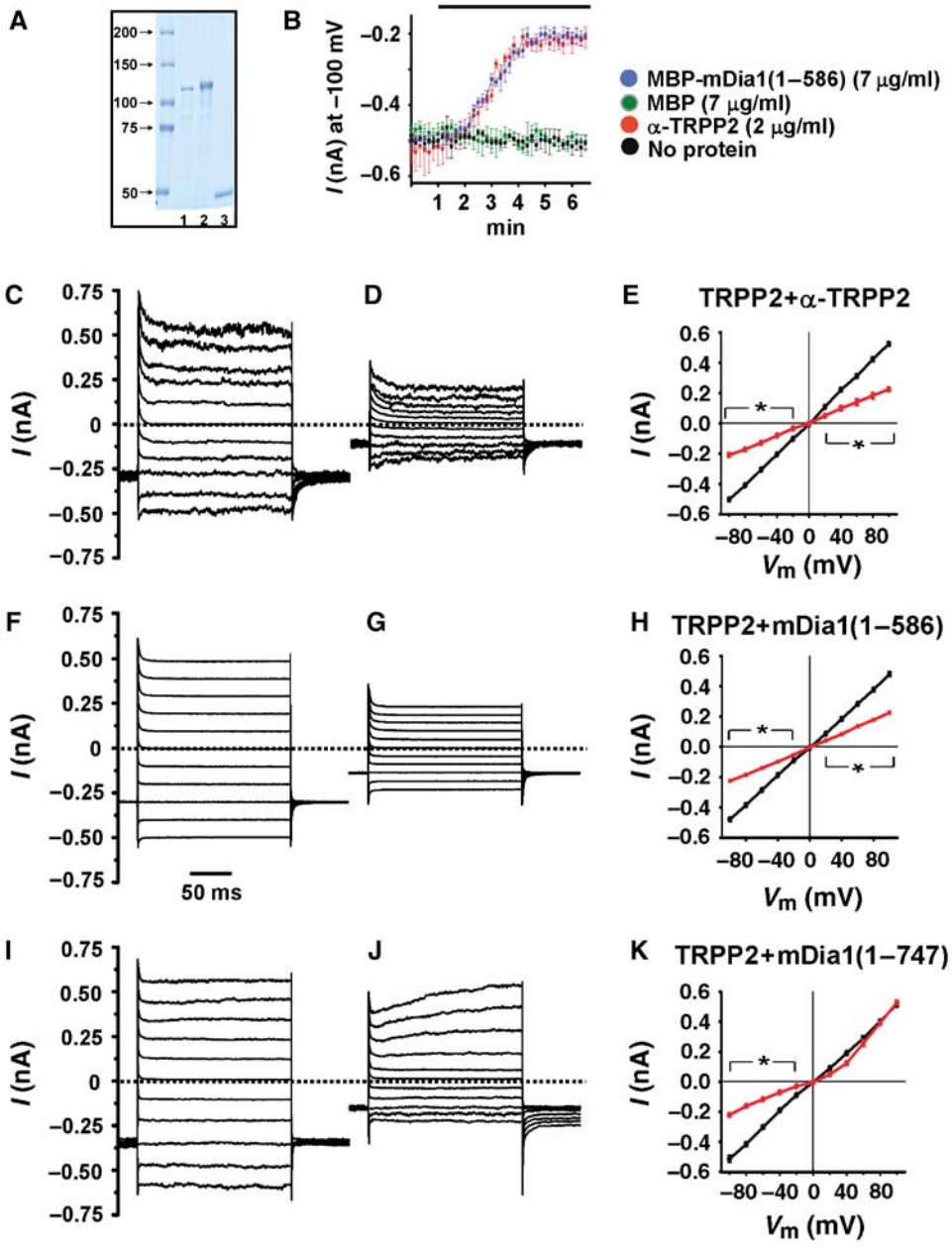

Figure 5 Voltage-dependent gating of TRPP2 by purified mDia1 in inside-out patches. (**A**) Coomassie blue staining of purified, recombinant MBP-mDia1(1–586) (lane 1), MBP-mDia1(1–747) (lane 2), or MBP (lane 3). (**B**) Time course of current inhibition by α-TRPP2 (2 μg/ml, $n=3$) (red) or recombinant MBP-mDia1(1–586) (7 μg/ml, $n=3$) (blue) applied directly to the bath solution in inside-out patches excised from LLC-PK1^{TRPP2} cells. Purified maltose-binding protein (MBP, 7 μg/ml, $n=3$) (green) or no protein (control, black) was used as negative controls. (**C**–**E**) Effect of bath application of α-TRPP2 on inside-out patches excised from LLC-PK1^{TRPP2} cells. Step currents before (C) and 5 min after (D) antibody application. (E) Pooled I–V curves before (black) and 5 min after (red) α-TRPP2 (2 μg/ml, $n=3$). (**F**–**H**) Effect of bath application of recombinant mDia1(1–586) on inside-out patches excised from LLC-PK1^{TRPP2} cells. Step currents before (F) and 5 min after (G) mDia1 (1–586) addition in the bath. (H) Pooled I–V curves before (black) and 5 min after (red) mDia1(1–586) (7 μg/ml, $n=6$). (**I**–**K**) Effect of bath application of recombinant mDia1(1–747) on inside-out patches excised from LLC-PK1^{TRPP2} cells. Step currents before (I) and 5 min after (J) mDia1(1–747) addition in the bath. (K) Pooled I–V curves before (black) and 5 min after (red) mDia1(1–747) (10 μg/ml, $n=5$). $^*P<0.05$.

voltage-independent action of this construct in excised patches. In sharp contrast, addition of recombinant mDia1(1–747) suppressed inward but not outward currents demonstrating a voltage-dependent effect of mDia1(1–747) on TRPP2 (Figure 5I–K). Consistently, mDia1(1–747) showed pronounced current relaxation and tail currents (Figure 5J) that were not seen in any of the patches incubated with α-TRPP2 or mDia1(1–586). It should be noted that the mDia1-dependent block of TRPP2 at negative potentials was irreversible for at least 5 min, following removal of recombinant mDia1 constructs from the bath (Supplementary Figure S7B–E).

EGF-induced activation of TRPP2 through mDia1-dependent gating

To determine the physiological relevance of the mDia1-dependent regulation of TRPP2, we tested whether it had an important function in its activation mechanism by EGF in LLC-PK1 cells. Such a role was suspected because EGF induced endogenous TRPP2 activity at hyperpolarizing potentials but not at depolarizing potentials (Ma *et al*, 2005). As activation of mDia1 requires activation of RhoA–C proteins, we tested whether EGF could activate endogenous RhoA in LLC-PK1 cells. Figure 6A and B shows the time-dependent activation of RhoA in response to EGF. Consistently, EGF

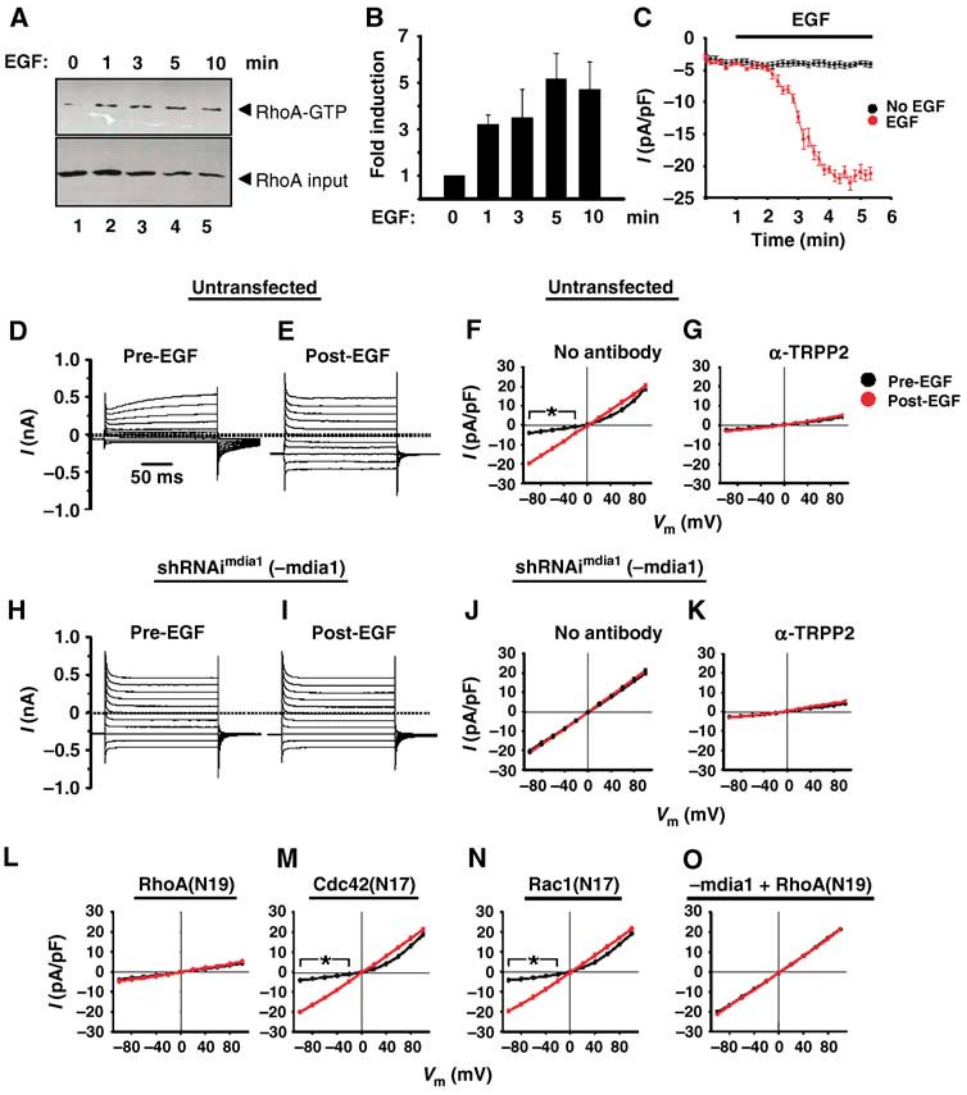

Figure 6 Activation of TRPP2 by EGF through mDia1-dependent gating. (**A**) Activation of RhoA by EGF in LLC-PK1 cells. Cells were activated by EGF (100 nM) and activated RhoA was pulled down by GST-Rhotekin (upper panel) at 0 (lane 1), 1 (lane 2), 3 (lane 3), 5 (lane 4), or 10 min (lane 5) following EGF addition. Activated RhoA (upper panel) or total RhoA (input, lower panel) was determined by immunoblotting with α-RhoA. (**B**) Summary data of EGF-induced activation of RhoA in LLC-PK1 cells from three independent experiments. (**C**) Time course of EGF-induced currents in native LLC-PK1 cells. Cells were incubated in the presence or absence of EGF (100 nM) for 5 min and whole cell currents at −100 mV were derived from voltage pulses from −60 to −100 mV for 200 ms applied every 10 s. Current reached maximum level 3 min following EGF addition to the bath solution. Step currents before (pre-EGF) (**D**) and 3 min after EGF (post-EGF) (100 nM) (**E**) in native LLC-PK1 (untransfected) cells. Pooled I–V curves before (pre-EGF, black, $n=8$) and after (post-EGF, red, $n=10$) EGF treatment in control LLC-PK1 cells (**F**) or same cells dialysed with 200 ng/ml of α-TRPP2 through the recording pipette ($n=8$) (**G**); $^*P<0.05$. Step currents before (**H**) and 3 min after EGF (100 nM) (**I**) in LLC-PK1 cells transiently transfected with shRNAi^{mDia1} (shRNAi^{mDia1} (−mDia1)). Pooled I–V curves before (black, $n=9$) and after (red, $n=9$) EGF treatment in LLC-PK1 cells transiently transfected with shRNAi^{mDia1} cells (**J**) or same cells dialysed with 200 ng/ml of α-TRPP2 through the recording pipette ($n=8$) (**K**). Pooled I–V curves before (pre-EGF, black) or 3 min after EGF (post-EGF, red) in LLC-PK1 transiently transfected with RhoA(N19), ($n=8$) (**L**), Cdc42(N17), ($n=8$) (**M**), Rac1(N17), ($n=8$) (**N**), or shRNAi^{mDia1} (−mDia1) plus RhoA(N19), $n=8$ (**O**).

activated an inward current with similar kinetics to RhoA activation (Figure 6C) in normal tyrode extracellular solution.

Next, basal (pre-EGF) and EGF-induced (post-EGF) conductance was measured in native LLC-PK1 cells (untransfected; Figure 6D–G) and LLC-PK1 cells transfected with shRNAi^{mDia1} (shRNAi^{mDia1}) (Figure 6H–K). Knock down of endogenous mDia1 caused an increase in inward currents that was almost identical in magnitude to the increase seen with EGF (compare Figure 6F red and J black). Moreover, EGF did not enhance further inward currents in cells lacking mDia1 (Figure 6J). EGF-induced or mDia1-knocked down-induced inward currents were carried by native TRPP2 because cell dialysis with α-TRPP2, but not control rabbit IgG or an irrelevant rabbit polyclonal α-CD8α, suppressed these currents (Figure 6G and K). These data showed that mDia1 was downstream of EGF in the activation of TRPP2 and led us to conclude that EGF signalled through mDia1 to activate TRPP2 by reversing the inhibitory effect of mDia1 on TRPP2.

To determine whether EGF activated mDia1 through RhoA, we tested whether a dominant-negative construct RhoA(N19) could suppress EGF-induced activation of TRPP2. Figure 6L shows that dominant-negative RhoA(N19) eliminated EGF-induced activation of TRPP2. The involvement of Rho proteins on TRPP2 activation was specific, as dominant-negative forms of other small GTPases such as Cdc42(N17) (Figure 6M) or Rac1(N17) (Figure 6N) did not have an effect. To test whether RhoA was upstream of mDia1 in the EGF-induced activation of TRPP2, we transiently co-transfected shRNAi^{mDia1} and RhoA(N19). Figure 6O shows that RhoA(N19) was ineffective in cells lacking mDia1. Therefore, RhoA functioned downstream of EGFR activation and upstream of mDia1 activation with regard to the EGF-induced activation of TRPP2.

Discussion

Our data indicate that native TRPP2 is part of a heteromultimeric channel complex existing in an inhibited state by binding to autoinhibited mDia1 at the resting membrane potential. However, this inhibition can be lifted by either membrane depolarization or EGF stimulation leading to channel activation. An important intermediary is RhoA, which functions upstream of mDia1 and downstream of membrane depolarization or EGFR activation (Figure 7). As a result, TRPP2 activation occurs through mDia1-dependent block/unblock.

TRPP2 functions as part of a heteromultimeric channel complex

Loss-of-function experiments in LLC-PK1 (Figure 2A and B) and other cell types (Pelucchi *et al*, 2006; Kim *et al*, 2008) consistently show that endogenous TRPP2 makes outwardly rectifying currents. However, massive TRPP2 overexpression (>10-fold) resulted in linear currents, which were at most ~50% larger in amplitude than native currents. Therefore, these data raised two interrelated questions. First, why massive TRPP2 overexpression failed to yield a proportional amplification of native TRPP2 currents, that is near 10-fold and second, why currents following TRPP2 overexpression lacked some residual outward rectification mediated by endogenous mDia1. We reasoned that TRPP2 cannot form a functional channel on its own, but it required other channel subunits, such as PKD1, TRPC1, TRPC4, and/or TRPV4, to assemble a minimal functional unit (Supplementary Figure S3F). This idea is well supported not only for TRPP2 (Hanaoka *et al*, 2000; Delmas *et al*, 2004; Bai *et al*, 2008) but also for other members of the TRPP subfamily, which are shown to function exclusively in a heteromultimeric manner

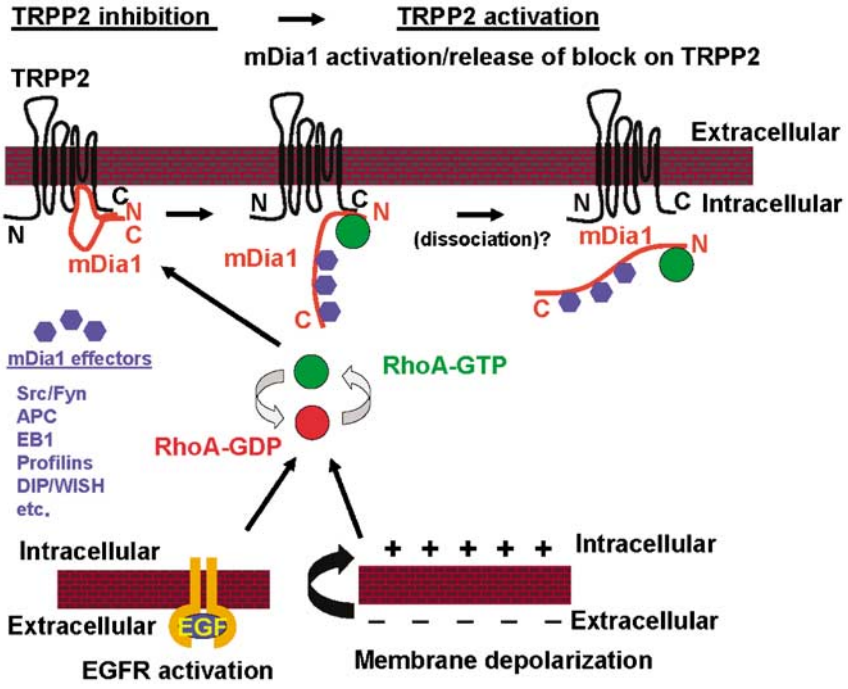

Figure 7 Proposed scheme of the mDia1-dependent regulation of TRPP2. At resting state (or hyperpolarizing potentials), TRPP2 (black) associates with the autoinhibited form of mDia1 (red), which blocks TRPP2 at these potentials. Membrane depolarization or EGF treatment induces the activation of RhoA from its GDP-bound state (red) to GTP-bound state (green). Activated RhoA (green) binds to and activates mDia1 resulting in the release of block and TRPP2 channel activation. mDia1 effector molecules (blue) bind to the activated form of mDia1.

(Huang *et al*, 2006; Ishimaru *et al*, 2006). PKD1, TRPC1, TRPC4, or TRPV4 are known direct or indirect interacting partners of TRPP2 (Tsiokas *et al*, 1997, 1999; Kottgen and Walz, 2005). Therefore, the ~50% increase in current amplitude can be explained by the limited amount of interacting channel subunits in these cells. With regard to the lack of residual outward rectification, we propose that massive overexpression of just TRPP2 could have stripped mDia1 from native TRPP2-containing complexes resulting in linear currents (Supplementary Figure S3F). Co-transfection experiments using tail current analysis confirmed this concept by showing that overexpression of constitutively active RhoA(V14) and mDia1 in LLC-PK1^{TRPP2} cells converted linear currents to outwardly rectifying currents. This concept was further supported by the converse experiment, whereby the amount of all interacting proteins was kept constant but TRPP2 was moderately overexpressed through the much weaker rat β-actin promoter. Moderate overexpression of TRPP2 resulted in native current amplification with outward rectification.

mDia1 regulates TRPP2 in a voltage-dependent manner

We show that native TRPP2, most likely in association with other channel subunits, displays voltage-dependent outward rectification, which is lost when mDia1 is knocked down. However, overexpressed TRPP2 makes linear currents, which become outwardly rectifying in the presence of activated mDia1. These data are consistent with previous descriptive data that native TRPP2 (Luo *et al*, 2003; Pelucchi *et al*, 2006; Kim *et al*, 2008), but not overexpressed TRPP2 alone (Ma *et al*, 2005) or in combination with PKD1 or TRPC1 (Hanaoka *et al*, 2000; Delmas *et al*, 2004; Bai *et al*, 2008), is voltage dependent. Therefore, we propose that mDia1 regulates TRPP2 activity in a voltage-dependent manner. We have shown previously that there is a physical interaction between TRPP2 and mDia1 (Rundle *et al*, 2004). On the basis of these lines of biochemical and functional evidence, it is tempting to speculate that mDia1 may form a voltage-dependent, intracellular gate for TRPP2 (Figure 7). However, we do not completely understand at the present time, the mechanism by which mDia1 confers voltage sensitivity on TRPP2. Experiments using the ΔN3mDia1 mutant in transfected cells and experiments in excised patches show that the effect of mDia1 on TRPP2 is direct and requires association of the two proteins. Specifically, ΔN3mDia1 has been shown to function as an activated form of mDia1 with regard to stress fiber formation and other cytoskeletal changes (Watanabe *et al*, 1999; Ishizaki *et al*, 2001). However, ΔN3mDia1 lacks the TRPP2-binding site. Therefore, if mDia1 had regulated TRPP2 through the cytoskeleton, ΔN3mDia1 should have indirectly affected TRPP2 activity, which was not the case. Direct effect of mDia1(1–586) or mDia1(1–747) on TRPP2 was most clearly shown in inside-out patches, whereby bath application of these constructs suppressed inward currents. Both of the constructs retained the TRPP2-binding site. In addition, mDia1(1–747), which was larger than mDia1 (1–586) by just the FH1 domain, functioned in a voltage-dependent manner. Therefore, if we were to speculate on the mechanism of action of mDia1 on TRPP2, we would like to propose the existence of three functional domains in mDia1: the TRPP2-binding domain, a domain up to residue 586 mediating the block on TRPP2, and the FH1/FH2 domains regulating voltage-dependent block/unblock of the second domain. It is currently unknown whether the second, blocking domain includes the TRPP2-binding domain. Further structure–function will be needed to fine map these domains.

The involvement of FH domains in the activation mechanism of TRPP2 has important implications in gating kinetics of TRPP2 by mDia1. There are numerous proteins/effectors known to associate with the activated form of mDia1 through FH domains (Wallar and Alberts, 2003). Therefore, it is very possible that binding of these proteins to activated mDia1 can regulate the rate of mDia1 activation itself, dwelling of activated mDia1 at the activated state, and/or mDia1-dependent activation of TRPP2 (Figure 7). This concept can explain differences in time constants in TRPP2 channel activation and deactivation based on the different systems used in our study. In native cells, a fixed stoichiometry between TRPP2, other channel subunits, mDia1, RhoA–C proteins, and/or mDia1 interacting proteins could dictate the activation kinetics of TRPP2. In overexpression systems, activation kinetics should be dictated, for the most part, by the overexpressed proteins. These differences can be further exemplified in excised patches where only fragments of mDia1 constructs were used in solution to study their effects in *trans*. Nevertheless, despite inherent differences within each system, all systems used in our study consistently showed that activated mDia1 had a voltage-dependent effect on TRPP2.

Activation of RhoA is downstream of membrane depolarization or EGF stimulation and upstream of mDia1-dependent activation of TRPP2

A prerequisite for the mDia1-mediated regulation of TRPP2 is mDia1 activation by RhoA–C proteins (Wallar and Alberts, 2003). Membrane depolarization has been shown to activate RhoA and its effector ROCK1 in a Ca^{2+}-dependent manner in excitable cells (Sakurada *et al*, 2003), whereas in a Ca^{2+}-independent manner in LLC-PK1 cells (Szaszi *et al*, 2005). Our data confirmed the depolarization-induced activation of RhoA, as overexpression of a dominant-negative mutant form of RhoA suppressed depolarization-induced activation of TRPP2 (Figure 6L, black). This effect was specific to RhoA as dominant-negative forms of Rac1 or Cdc42 did not affect native TRPP2 currents and mediated through mDia1. Consistently, TRPP2 overexpression escaped depolarization-induced regulation by native RhoA. Therefore, these data provide a mechanistic explanation for the depolarization-induced activation of native TRPP2 through the activation of RhoA (Figure 7).

We show that mDia1-dependent gating served as an obligatory step in its activation by EGF, and possibly other signal transduction pathways that would result in the activation of RhoA. The effect of EGF on TRPP2 was specific to RhoA as overexpression of dominant-negative forms of two other small GTPases, Cdc42(N17) or Rac1(N17) was without effect. The activation of RhoA by EGF was demonstrated by a classical Rhotekin assay and was consistent with previous reports that receptor tyrosine kinases activated RhoA, Rac1, and Cdc42 in other systems (Liu and Burridge, 2000; Tybulewicz, 2005). However, the RhoA/mDia1 limb of the pathway was particularly relevant to our study, as mDia1 is a specific effector of Rho proteins (A–C) and not of Rac1 or Cdc42 (Watanabe *et al*, 1997). We have previously shown

that EGF activation of TRPP2 involved the PLC/PI3K/PIP_2 pathway, as pharmacological manipulation of this pathway strongly affected EGF-induced activation of TRPP2 (Ma *et al*, 2005). Although the previous studies were carried out in overexpressed TRPP2, it would be interesting to investigate in the future how the PLC/PI3K/PIP_2 pathway affects endogenous TRPP2 activation by EGF, and how RhoA/mDia1 interface with the PLC/PI3K/PIP_2 pathway.

Overall, we provide evidence for a new role of mDia1 in the direct, voltage-dependent regulation of TRPP2. This type of regulation can couple Rho-dependent signal transduction cascades to Ca^{2+} signalling and translate cytsoskeletal and other RhoA/mDia1-mediated processes to changes in intracellular Ca^{2+} concentration.

Materials and methods

Indirect immunofluorescence

LLPCK1 cells were grown to 60% confluence on glass cover slips. In experiments involving GSK3 inhibition, cells were treated for 16 h with 40 μM SB 415286 (Tocris Bioscience, Ellisville, MO, USA) before fixation. Cells were fixed with ice-cold methanol/acetone (70:30) at 4°C for 10 min followed by air drying for 10 min. Blocking was carried out for 15 min with 5% bovine serum albumin in phosphate-buffered saline (BSA/PBS). Cells were incubated with a goat polyclonal anti-TRPP2 antibody G20 (Santa Cruz Biotechnology Inc.) overnight at 4°C in 1% BSA/PBS (1:50 dilution). Antibody binding was visualized using a FITC-conjugated donkey anti-goat IgG secondary antibody (Santa Cruz Biotechnology Inc.). Slides were viewed using an Olympus Imaging Systems inverted IX71 microscope configured for multi-fluorescence image capture. Images were acquired and analysed using SimplePCI imaging software (Compix Inc.) (Figure 1A and B). Double staining (Figure 1D and E) was performed as described above but with the inclusion of a 5-min incubation with 0.2% Triton X-100 in PBS following fixation. Detection of TRPP2 and mDia1 was carried out by α-TRPP2 (1:50, G20) and mouse monoclonal α-mDia1 (1:500; BD Biosciences-Pharmingen), respectively. Primary antibodies were detected by Alexa 568-conjugated donkey anti-goat and Alexa 488-conjugated donkey goat anti-mouse secondary antibodies (1:2000). Images were captured by a Leica SP2 MP confocal system. An average of 11 *z*-sections is shown in Figure 1D–F.

Electrophysiology

The conventional whole cell voltage-clamp configuration was used to measure transmembrane currents in single cells. Patch-clamp recordings were obtained from single cells at room temperature using a Warner PC-505B amplifier (Warner Instrument Corp., Hamden, CT, USA) and pClamp 8 software (Axon Instrument, Foster City, CA, USA). Glass pipettes (plain; Fisher Scientific, Pittsburgh, PA, USA) with resistances of 5–8 MΩ were prepared with a pipette puller and polisher (PP-830 and MF-830, respectively; Narishige, Tokyo, Japan). After the whole cell configuration was achieved, cell capacitance and series resistance (10–12 MΩ) were compensated by 70–80% before each recording period. From a holding potential of −60 mV, voltage steps were applied from −100 to 100 mV in 20 mV increments with 200 ms duration at 3-s intervals. To obtain tail currents, cells were held at −60 mV, prepulsed at 120 mV for 200 ms and voltage steps were applied from −160 to 120 mV in 20 mV increments with 200 ms duration at 3-s intervals. Current traces were filtered at 1 kHz and analysed off-line with pClamp 8. Statistical analysis was employed with the SigmaStat software (Chicago, IL, USA). Data were reported as means ± s.e.m. Student's *t*-test was used for comparisons between groups. Differences were considered significant when $P<0.05$. The pipette solution contained (in mM): 100 K-aspartate, 30 KCl, 0.3 Mg-ATP, 10 HEPES, 10 EGTA, and 0.03 GTP (pH 7.2). The extracellular solution was normal tyrode solution containing (in mM): 135 NaCl, 5.4 KCl, 0.33 NaH_2PO_4, 1 $MgCl_2$, 1.8 $CaCl_2$, 5 HEPES, 5.5 glucose (pH 7.4) or symmetrical K^+ containing (in mM): 130 KCl, 1 $MgCl_2$, 10 HEPES, 0.1 $CaCl_2$, and 5 glucose (pH 7.4). EGF (100 nM)-induced whole cell currents were measured 3 min after the addition of EGF to the bath solution. In experiments using cell dialysis with antibodies, recordings were made 5 min after break-in to allow sufficient time for antibody diffusion into the cell, except for measurements of membrane potential in experiments in LLC-PK1 cells (Figure 2I). The Boltzmann equation used to plot conductance as a function of voltage and calculate G_{max} was as follows: $y = A_1 - A_2/1 + e^{(x-x_o)/dx} + A_2$, where y is the conductance (G) at a given voltage (x), A_1 and A_2 are the G_{max} and G_{min}, respectively, x is the given voltage, x_o is the $V_{1/2}$, and dx is the slope factor. Microcal Origin 6.0 software was used to fit the data.

Macroscopic currents in inside-out patches were measured according to Hamill *et al* (1981). Pipette resistance was 1–3 MΩ and excised patches were air-exposed for 2 s before recordings. Voltage applied through the pipette (V_p) was +60 mV, which corresponded to −60 mV of the whole cell configuration and used as the holding potential (V_h). Time-course data (Figure 5B) were derived by voltage pulses from $V_h = -60$ to −100 mV applied every 10 s. Voltage steps were delivered from −60 mV and covered a range from −100 to 100 mV with 20 mV increments and pulse duration of 200 ms. The pipette solution contained (in mM): 130 KCl, 1 $MgCl_2$, 10 HEPES, 0.1 $CaCl_2$, and 5 glucose (pH 7.4) plus 50 μM niflumic acid to block Cl^- currents. The bath solution contained (in mM): 100 K-aspartate, 30 KCl, 0.3 Mg-ATP, 10 HEPES, 10 EGTA, and 0.03 GTP (pH 7.2).

Measurement of resting membrane potential

At 48 h following transfection (LLC-PK1 cells), CD8α-expressing cells were identified by a brief incubation with CD8-coated beads and the resting membrane potential was determined by a gap-free protocol using current clamp. The pipette solution contained (in mM): 140 KCl, 2 $MgCl_2$, 3 Na_2ATP, 0.1 GTP, 5 HEPES, and 5 EGTA, pH 7.2. Extracellular solution was normal tyrode solution. Recordings were filtered at 5 kHz and initiated immediately after break-in to demonstrate a time-dependent effect of antibody infusion into the cell.

Supplementary data

Supplementary data are available at *The EMBO Journal* Online (http://www.embojournal.org).

Acknowledgements

We thank Drs Shuh Narumiya for GFP-mDia1 and GFP-ΔN3mDia1 and Reinhold Penner and Hamid Akbarali for comments on the paper. This study was supported by the Wellcome Trust (ACMO, GR071201), Research Councils UK (AJS), PKD Foundation, OCAST, NIH (DK59599), and the John S Gammill Endowment in PKD (LT).

References

Bai CX, Giamarchi A, Rodat-Despoix L, Padilla F, Downs T, Tsiokas L, Delmas P (2008) Formation of a new receptor-operated channel by heteromeric assembly of TRPP2 and TRPC1 subunits. *EMBO Rep* 2008; e-pub ahead of print 7 March 2008; doi:10.1038/embor.2008.29

Cantiello HF (2004) Regulation of calcium signaling by polycystin-2. *Am J Physiol Renal Physiol* **286:** F1012–F1029

Delmas P, Nauli SM, Li X, Coste B, Osorio N, Crest M, Brown DA, Zhou J (2004) Gating of the polycystin ion channel signaling complex in neurons and kidney cells. *FASEB J* **18:** 740–742

Gonzalez-Perrett S, Batelli M, Kim K, Essafi M, Timpanaro G, Moltabetti N, Reisin IL, Arnaout MA, Cantiello HF (2002) Voltage dependence and pH regulation of human polycystin-2-mediated cation channel activity. *J Biol Chem* **277:** 24959–24966

Gonzalez-Perrett S, Kim K, Ibarra C, Damiano AE, Zotta E, Batelli M, Harris PC, Reisin IL, Arnaout MA, Cantiello HF (2001) Polycystin-2, the protein mutated in autosomal dominant polycystic kidney disease (ADPKD), is a Ca^{2+}-permeable

nonselective cation channel. *Proc Natl Acad Sci USA* **98:** 1182–1187

Gundersen GG, Gomes ER, Wen Y (2004) Cortical control of microtubule stability and polarization. *Curr Opin Cell Biol* **16:** 106–112

Hamill OP, Marty A, Neher E, Sakmann B, Sigworth FJ (1981) Improved patch-clamp techniques for high-resolution current recording from cells and cell-free membrane patches. *Pflugers Arch* **391:** 85–100

Hanaoka K, Qian F, Boletta A, Bhunia AK, Piontek K, Tsiokas L, Sukhatme VP, Guggino WB, Germino GG (2000) Co-assembly of polycystin-1 and -2 produces unique cation-permeable currents. *Nature* **408:** 990–994

Higgs HN (2005) Formin proteins: a domain-based approach. *Trends Biochem Sci* **30:** 342–353

Huang AL, Chen X, Hoon MA, Chandrashekar J, Guo W, Trankner D, Ryba NJ, Zuker CS (2006) The cells and logic for mammalian sour taste detection. *Nature* **442:** 934–938

Ishimaru Y, Inada H, Kubota M, Zhuang H, Tominaga M, Matsunami H (2006) Transient receptor potential family members PKD1L3 and PKD2L1 form a candidate sour taste receptor. *Proc Natl Acad Sci USA* **103:** 12569–12574

Ishizaki T, Morishima Y, Okamoto M, Furuyashiki T, Kato T, Narumiya S (2001) Coordination of microtubules and the actin cytoskeleton by the Rho effector mDia1. *Nat Cell Biol* **3:** 8–14

Kim I, Fu Y, Hui K, Moeckel G, Mai W, Li C, Liang D, Zhao P, Ma J, Chen XZ, George Jr AL, Coffey RJ, Feng ZP, Wu G (2008) Fibrocystin/polyductin modulates renal tubular formation by regulating polycystin-2 expression and function. *J Am Soc Nephrol* **19:** 455–468

Kottgen M, Walz G (2005) Subcellular localization and trafficking of polycystins. *Pflugers Arch* **451:** 286–293

Koulen P, Cai Y, Geng L, Maeda Y, Nishimura S, Witzgall R, Ehrlich BE, Somlo S (2002) Polycystin-2 is an intracellular calcium release channel. *Nat Cell Biol* **4:** 191–197

Lammers M, Rose R, Scrima A, Wittinghofer A (2005) The regulation of mDia1 by autoinhibition and its release by Rho*GTP. *EMBO J* **24:** 4176–4187

Li Q, Montalbetti N, Shen PY, Dai XQ, Cheeseman CI, Karpinski E, Wu G, Cantiello HF, Chen XZ (2005a) Alpha-actinin associates with polycystin-2 and regulates its channel activity. *Hum Mol Genet* **14:** 1587–1603

Li Y, Wright JM, Qian F, Germino GG, Guggino WB (2005b) Polycystin 2 interacts with type I inositol 1,4,5-trisphosphate receptor to modulate intracellular Ca^{2+} signaling. *J Biol Chem* **280:** 41298–41306

Liu BP, Burridge K (2000) Vav2 activates Rac1, Cdc42, and RhoA downstream from growth factor receptors but not beta1 integrins. *Mol Cell Biol* **20:** 7160–7169

Luo Y, Vassilev PM, Li X, Kawanabe Y, Zhou J (2003) Native polycystin 2 functions as a plasma membrane Ca^{2+}-permeable cation channel in renal epithelia. *Mol Cell Biol* **23:** 2600–2607

Ma R, Li WP, Rundle D, Kong J, Akbarali HI, Tsiokas L (2005) PKD2 functions as an epidermal growth factor-activated plasma membrane channel. *Mol Cell Biol* **25:** 8285–8298

Mochizuki T, Wu G, Hayashi T, Xenophontos SL, Veldhuisen B, Saris JJ, Reynolds DM, Cai Y, Gabow PA, Pierides A, Kimberling WJ, Breuning MH, Deltas CC, Peters DJ, Somlo S (1996) PKD2, a gene for polycystic kidney disease that encodes an integral membrane protein. *Science* **272:** 1339–1342

Narumiya S, Yasuda S (2006) Rho GTPases in animal cell mitosis. *Curr Opin Cell Biol* **18:** 199–205

Nilius B, Owsianik G, Voets T, Peters JA (2007) Transient receptor potential cation channels in disease. *Physiol Rev* **87:** 165–217

Nilius B, Talavera K, Owsianik G, Prenen J, Droogmans G, Voets T (2005) Gating of TRP channels: a voltage connection? *J Physiol* **567:** 35–44

Otomo T, Otomo C, Tomchick DR, Machius M, Rosen MK (2005) Structural basis of Rho GTPase-mediated activation of the formin mDia1. *Mol Cell* **18:** 273–281

Pelucchi B, Aguiari G, Pignatelli A, Manzati E, Witzgall R, Del Senno L, Belluzzi O (2006) Nonspecific cation current associated with native polycystin-2 in HEK-293 cells. *J Am Soc Nephrol* **17:** 388–397

Rose R, Weyand M, Lammers M, Ishizaki T, Ahmadian MR, Wittinghofer A (2005) Structural and mechanistic insights into the interaction between Rho and mammalian Dia. *Nature* **435:** 513–518

Rundle DR, Gorbsky G, Tsiokas L (2004) PKD2 interacts and co-localizes with mDia1 to mitotic spindles of dividing cells: role of mDia1 IN PKD2 localization to mitotic spindles. *J Biol Chem* **279:** 29728–29739

Sakurada S, Takuwa N, Sugimoto N, Wang Y, Seto M, Sasaki Y, Takuwa Y (2003) Ca^{2+}-dependent activation of Rho and Rho kinase in membrane depolarization-induced and receptor stimulation-induced vascular smooth muscle contraction. *Circ Res* **93:** 548–556

Scheffers MS, Le H, van der Bent P, Leonhard W, Prins F, Spruit L, Breuning MH, de Heer E, Peters DJ (2002) Distinct subcellular expression of endogenous polycystin-2 in the plasma membrane and Golgi apparatus of MDCK cells. *Hum Mol Genet* **11:** 59–67

Streets AJ, Moon DJ, Kane ME, Obara T, Ong AC (2006) Identification of an N-terminal glycogen synthase kinase 3 phosphorylation site which regulates the functional localization of polycystin-2 *in vivo* and *in vitro*. *Hum Mol Genet* **15:** 1465–1473

Szaszi K, Sirokmany G, Di Ciano-Oliveira C, Rotstein OD, Kapus A (2005) Depolarization induces Rho-Rho kinase-mediated myosin light chain phosphorylation in kidney tubular cells. *Am J Physiol Cell Physiol* **289:** C673–C685

Threadgill DW, Dlugosz AA, Hansen LA, Tennenbaum T, Lichti U, Yee D, LaMantia C, Mourton T, Herrup K, Harris RC, Barnard JA, Yuspa SH, Coffey RJ, Magnuson T (1995) Targeted disruption of mouse EGF receptor: effect of genetic background on mutant phenotype. *Science* **269:** 230–234

Tsiokas L, Arnould T, Zhu C, Kim E, Walz G, Sukhatme VP (1999) Specific association of the gene product of PKD2 with the TRPC1 channel. *Proc Natl Acad Sci USA* **96:** 3934–3939

Tsiokas L, Kim E, Arnould T, Sukhatme VP, Walz G (1997) Homo- and heterodimeric interactions between the gene products of PKD1 and PKD2. *Proc Natl Acad Sci USA* **94:** 6965–6970

Tsiokas L, Kim S, Ong EC (2007) Cell biology of polycystin-2. *Cell Signal* **19:** 444–453

Tybulewicz VL (2005) Vav-family proteins in T-cell signalling. *Curr Opin Immunol* **17:** 267–274

Vassilev PM, Guo L, Chen XZ, Segal Y, Peng JB, Basora N, Babakhanlou H, Cruger G, Kanazirska M, Ye C, Brown EM, Hediger MA, Zhou J (2001) Polycystin-2 is a novel cation channel implicated in defective intracellular Ca(2+) homeostasis in polycystic kidney disease. *Biochem Biophys Res Commun* **282:** 341–350

Venkatachalam K, Montell C (2007) TRP channels. *Annu Rev Biochem* **76:** 387–417

Voets T, Droogmans G, Wissenbach U, Janssens A, Flockerzi V, Nilius B (2004) The principle of temperature-dependent gating in cold- and heat-sensitive TRP channels. *Nature* **430:** 748–754

Wallar BJ, Alberts AS (2003) The formins: active scaffolds that remodel the cytoskeleton. *Trends Cell Biol* **13:** 435–446

Watanabe N, Kato T, Fujita A, Ishizaki T, Narumiya S (1999) Cooperation between mDia1 and ROCK in Rho-induced actin reorganization. *Nat Cell Biol* **1:** 136–143

Watanabe N, Madaule P, Reid T, Ishizaki T, Watanabe G, Kakizuka A, Saito Y, Nakao K, Jockusch BM, Narumiya S (1997) p140mDia, a mammalian homolog of *Drosophila* diaphanous, is a target protein for Rho small GTPase and is a ligand for profilin. *EMBO J* **16:** 3044–3056

Wu G, Markowitz GS, Li L, D'Agati VD, Factor SM, Geng L, Tibara S, Tuchman J, Cai Y, Park JH, van Adelsberg J, Hou Jr H, Kucherlapati R, Edelmann W, Somlo S (2000) Cardiac defects and renal failure in mice with targeted mutations in Pkd2. *Nat Genet* **24:** 75–78

